Title

Enhanced damage localization for complex structures through statistical modeling and sensor fusion

Authors

Haynes, Colin
Todd, Michael

Publication Date

2015-03-01

DOI

10.1016/j.ymssp.2014.08.015

Peer reviewed

Enhanced Damage Localization for Complex Structures through Statistical Modeling and Sensor Fusion

Colin Haynes[a] and Michael Todd*[a]

[a]Department of Structural Engineering, UC San Diego
9500 Gilman Drive, La Jolla, CA 92093

* Corresponding author, mdtodd@ucsd.edu, (858) 534-5951

Abstract

Ultrasonic guided waves represent a promising technique for detecting and localizing structural damage, but their application to realistic structures has been hampered by the complicated interference patterns produced by scattering from geometric features. This work presents a new damage localization paradigm based on a statistical approach to dealing with uncertainty in the guided wave signals. A bolted frame and a section of a fuselage rib are tested with different simulated damage conditions and used to conduct a detailed comparison between the proposed solution and other sparse-array localization approaches. After establishing the superiority of the statistical approach, two novel innovations to the localization procedure are proposed: an approach to sensor fusion based on the Neyman-Pearson criterion, and a method of constructing simple models of geometrical features. Including the sensor fusion and geometrical models produces a substantial improvement in the system's localization accuracy. The final result is a robust and accurate framework for single-site damage localization that moves structural health monitoring towards practical implementation on a much broader range of structures.

Keywords:

Damage localization, ultrasonic guided waves, sensor fusion, statistical modeling, complex structures, structural health monitoring

1. Introduction

Within the paradigm of structural health monitoring (SHM), there exists a hierarchy of information about a structure's state that may be exploited in order to provide a meaningful diagnosis and thereby make well-informed decisions about performance, maintenance, or operational fitness [1]. The most basic SHM systems provide some form of indication about whether the structure has become damaged, based upon pre-established definitions of the target damage resulting from an operational evaluation of the system. The next question following that of existence is the question of location of the damage. Damage extent and type would then be addressed, finally leading to a damage prognosis assessment, the ultimate goal for practical implementation of SHM systems [2].

In order to begin considering the answers to these questions, a particular inspection technology must be selected based on the parameters of the system to be monitored. In this study, ultrasonic guided waves (UGWs) sent and received by a sparse array of piezoelectric transducers are the mechanism for extracting damage information. Sparse array techniques can provide excellent coverage area per sensor, thus offering cost and weight savings over methods utilizing denser configurations [3]. In this paper, UGW interrogation is applied to testbeds of significant geometric complexity, including bolted connections, through-holes, stringers, boundaries, and other geometric features. One of the chief difficulties with UGW interrogation has been that any geometric feature causes the waves to scatter (often in a manner similar to a target defect). The resulting multitude of reflections often creates complex, multi-path interference patterns, making the waveforms difficult to interpret. Techniques specifically developed for problems of a realistic level of complexity are needed in order to transition SHM systems to real-world applications.

The present work focuses only on the damage localization problem, or the second step in the SHM decision hierarchy which assumes that the more basic question “Is damage present?” has been answered affirmatively in a global sense. An optimal approach to the purely damage detection problem has been presented previously for the same testbeds [4]. Therefore, the fundamental objective of this paper is to develop methods that will most accurately predict the location of single-site damage on complex structures given that the damage exists.

In this study, a statistical approach is utilized to determine first-arrival time-of-flight information for sparse arrays on two distinct and geometrically-complex testbeds – a bolted frame structure and a fuselage rib aircraft component. The statistical approach, which was presented previously for a notably simpler structure [5], is extended to the more complex testbeds considered here. The results not only demonstrate the robustness of the approach to specific structure and (simulated) damage types, but also confirm its superior localization performance compared to a representative selection of other localization algorithms in the literature. To further enhance the localization accuracy, two novel techniques are developed and implemented: a sensor fusion approach based on the Neyman-Pearson criterion and a simple modeling approach for the most significant geometric features. The integrated localization approach, considering sensor fusion and modeling techniques, provides excellent localization accuracy for highly-complex structures and represents a significant step toward the implementation of viable SHM systems.

2. Localization Strategy

Most sparse ultrasonic sensor arrays in the SHM field utilize the method of delay-and-sum beamforming as the basis of determining the damage location [6–8]. In this method, reflectors are located by launching a pulse into the medium from one transducer and receiving the waveform at another transducer. Through knowledge of the wave velocity, sensor locations, and actuation time, the time of arrival of the first reflected wave packet (or “first arrival”) can be translated into the total distance from actuator to reflector to receiver. Most often, it is the residual signal—the signal resulting from a baseline subtraction procedure—that is considered, in order to reduce (ideally, to remove entirely) the influence of the direct arrival between sensors and any reflections from any benign structural features. The optimal baseline subtraction procedure is used in this study, as a straightforward technique to also minimize the impact of any changes in environmental condition by subtracting the baseline taken in the nearest environmental state, and thereby localize only damage-related reflections [9].

Because realistic structures tend to be more geometrically complex than a uniform plate, reflected damage signals quickly become obscured by reflections from benign geometric features. While appropriate baseline subtraction can help mitigate the effect of these features, all of the echoes from any damage will likewise scatter from the geometric features, causing the residual signal to become substantially more complicated as well. As a result, many adaptations to the delay-and-sum technique have been proposed. A representative selection of these techniques has been implemented in order to compare the proposed solution with those existing in the literature. The details of each localization algorithm are presented in the “Localization Results” section.

However, in this work structures with a high level of geometric complexity are specifically targeted. These structures present challenges that lend themselves to a statistical formulation given the uncertainty imposed by the complexity. Therefore, a maximum likelihood estimation (MLE) approach presented previously is used as an "arrival filter" to compute the likelihood that any given point in the time series of a particular sensor pair is the true first arrival point [5]. The key assumptions of this approach are as follows: before the first arrival, the enveloped residual signal may be described by a Rayleigh-distributed random process. After the first arrival (due to the complex, overlapping echoes of waves reflected from the damage), the signal may be described as a Raleigh-distributed random process with a greater Rayleigh parameter. Computing the maximum likelihood estimate of each of the two Rayleigh parameters, a likelihood ratio test can be implemented to describe the likelihood that each time point is the first arrival. Because the maximum of the resulting vector is the predicted arrival point, the output of this filter may then be used in a delay-and sum procedure to produce a predicted damage location in the structure.

There are some other key assumptions that go into the first-arrival estimation procedure. First, as is common to all delay-and-sum formulations, this approach assumes single-mode propagation. That is, one mode is dominantly actuated and received by the sensor array, and this mode has a known group velocity. The velocity in both of these structures has been estimated from the time of flight of the direct arrivals (without baseline subtraction) and the known distance between sensors. The final values consist of the average of the velocities estimated from all tests and most sensor pairs (excluding sensor pairs too far apart to receive direct arrivals and, in the fuselage rib, those with direct line-of-sight obstructions). The final values obtained are 2120 m/s for the frame structure and 5450 m/s for the fuselage rib structure. This procedure deliberately estimates an "effective" or *in situ* group velocity, which represents the speed at which energy actually propagates between sensors and requires no detailed wave propagation models of the medium. Because in guided wave SHM, the frequency and wave mode are usually chosen to avoid the most highly dispersive situations, using the estimated, *in situ* velocity is enough of a robust approach to be effectual without the need for any explicit dispersion compensation model.

Furthermore, the fundamental premise of the estimation is that the signal is broken into two sections– before and after the first arrival of a significant damage reflection. Thus, the method inherently assumes that sensor pairs at arbitrary locations are actually able to observe damage reflections—that is, the amplitude of the first arriving wave (and the subsequent reflections) should be greater than the noise floor in a quantifiable sense. However, the impact of sensor pairs not observing the damage can be mitigated with proper application of sensor fusion principles. The damage modes considered here are not particularly directional, so the assumption of damage observability effectively replaces detailed models of scattering behavior (although such models could still be utilized with the proposed methodology).

This study is concerned only with point-like scatterers assumed to occur at one location. Should multiple-site damage be of interest, it is possible the MLE approach could be modified to take this into account. The fundamental premise of the approach is that the first arrival is identified by the many, overlapping echoes that follow, so if the damage modes are separated by enough distance that they are

observed by different sensor pairs, both sites may be evident in the delay-and-sum result. Damage sites closer together or damage modes covering a larger area would be expected to cause maxima at each edge, depending on the direction of the incoming waves. Thus, while it seems theoretically possible that this approach could be extended to multiple damage locations or even damage modes covering a larger area, such damage modes are outside the scope of the present study.

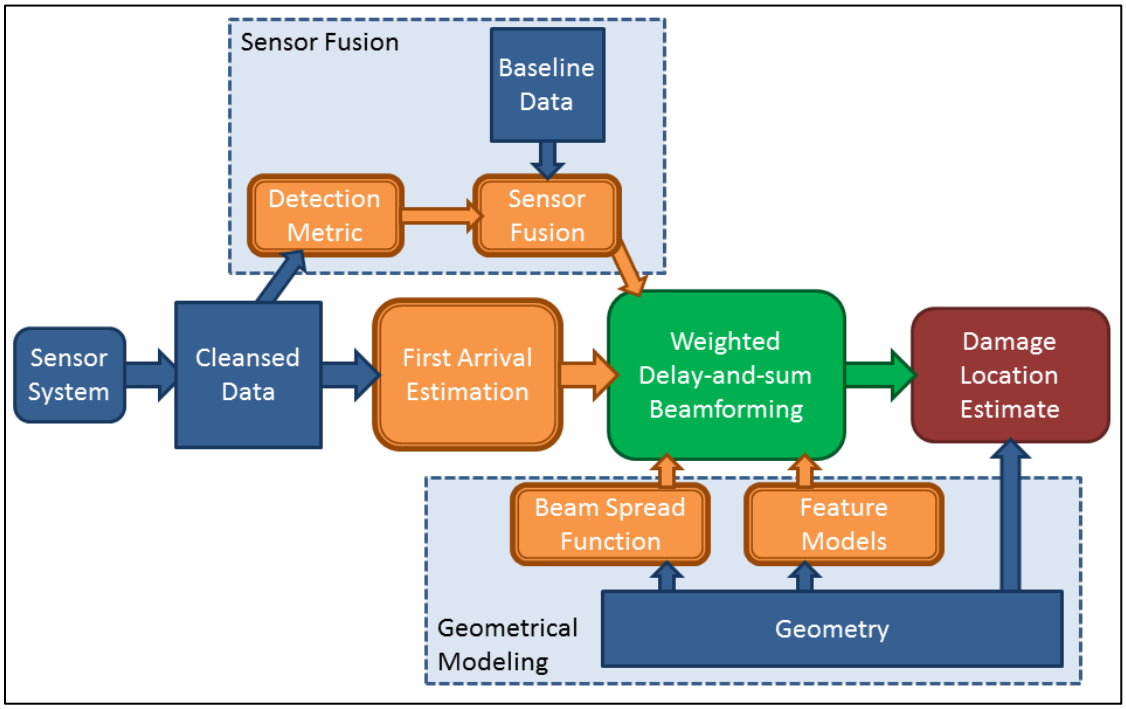

Figure 1 - Flowchart of general localization architecture. Data are represented by nodes with square corners; processes are represented by nodes with rounded corners.

Figure 1 shows a visual representation of the overall processing procedure used in the proposed paradigm. The process begins with the data being collected on the left and moves all the way to the damage location estimate on the right. The "Cleansed Data" box refers to the data after filtering, baseline subtraction, and enveloping procedures are applied. Each of the orange, double-lined nodes in the figure represents a step where one of various techniques may be chosen to enhance the SHM system performance. The central element of the process is the weighted delay-and-sum beamforming step, which takes as inputs the estimated first arrival points and weights from the sensor fusion technique, beam spread function, and feature models. Each of those steps is discussed in this study, with the exception of the feature computation step which was addressed previously [4]. The beam spread function and feature modeling steps are based on the geometry of the system and are grouped accordingly. The sensor fusion procedure is described in the next section and relies on information from the detection process in order to supplement the localization process. The objective of this work, therefore, is to demonstrate a comprehensive methodology for damage location prediction from UGW SHM systems on complex structures. The next section, therefore, will describe the selecting approaches for each of the modeling steps.

3. Sensor Fusion and Modeling Approach

3.1. Sensor Fusion

Sensor fusion refers to the process of integrating data from multiple sensors in a way that enhances the decision-making performance of the system. The sensor fusion process takes the full data matrix (which has a size corresponding to the number of time samples by the number of sensor pairs by the number of trials) and reduces it down to a form where a decision can be made. Each trial represents one full round of data acquisition (including averaging if used), each with an independent damage state. Thus, in the context of detection, the fusion result usually consists of a one-dimensional vector (with a length corresponding to the number of trials) to which a threshold value may be applied to decide the damage state estimates. In the present context of localization, the data must undergo the further step of transformation through the wave velocity from the time domain to the spatial domain in order to estimate the damage location.

Hall [10] gives a good overview of the general sensor fusion process along with many application examples. Liu and Wang [11] proposed a three-level hierarchy of different sensor fusion methods, where the three levels are data-level, feature-level, and decision-level. Data-level fusion refers to combining raw data from sensors directly. Feature-level fusion involves performing the feature extraction (i.e., applying the appropriate detector) on each sensor pair individually and then combining the features to make the decision. Decision-level fusion is the highest-level fusion – all sensors make a decision independently, and the results from their decisions are then fused. This hierarchical view was subsequently applied to guided wave SHM by Lu and Michaels [12]. Haynes *et al*. [4] compared many different fusion techniques from the literature and their effect on detection performance for the same experimental data used here.

The form of fusion proposed for the present localization paradigm is based on decision-level fusion. Because decisions are made on a sensor-by-sensor basis, more information is available for the delay-and-sum procedure. For large enough structures instrumented with a sparse array, damage in arbitrary locations does not cause significant changes in the signal between some of the sensor pairs, which causes the maximum-likelihood estimate of the first arrival to break down. Therefore, the Neyman-Pearson (NP) criterion is applied to the signal from each sensor pair separately and only the sensors that detect the presence of damage are utilized. This method will be referred to as “NP binary fusion”. Much the same approach has been proposed by Niri *et al*. [13] in the context of acoustic emission. The sensor-level damage detection procedure follows that laid out previously (in a study using the same data sets), utilizing the normalized residual energy (NRE) as the theoretically-optimal damage detection metric for systems with minimal *a priori* knowledge and high signal complexity [4]. Equation (1) gives the equation for calculating the NRE values (denoted as **E**) for each sensor pair *i* and *j*, based on the baseline-subtracted residual signals **x** and the filtered, baseline signals **y**.

$$\mathbf{E}_{ij} = 20 * \log_{10}\left[\frac{\sum_n \mathbf{x}_{ij}^2[n]}{\sum_n \mathbf{y}_{ij}^2[n]}\right] \tag{1}$$

Next, the threshold values for each sensor pair (denoted as **T**) are computed by taking the maximum across all of the undamaged trials as shown in Equation (2). The index (*k*) represents the different trials.

$$\mathbf{T}_{ij} = \max\left(\mathbf{E}_{ij}^{(k)},\ \forall\ \mathbf{E}^{(k)} \in \text{undamaged}\right) \tag{2}$$

Then the NRE values are compared to the thresholds to form **D**:

$$\mathbf{D}_{ij} \equiv 10^{\left(\mathbf{E}_{ij} - \mathbf{T}_{ij}\right)/20} \tag{3}$$

Finally, the scaling factor of each pair, **S**, is set to one for all pairs that exceed the threshold and zero otherwise:

$$\mathbf{S}_{ij}^{\text{NP binary}} = \begin{cases} 1,\ \mathbf{D}_{ij} > 1 \\ 0,\ \mathbf{D}_{ij} \le 1 \end{cases} \tag{4}$$

Increasing the sophistication by one more step, the contribution of each sensor pair to the delay-and-sum procedure can be scaled by a factor proportional to the confidence that the sensor pair can observe the damage. Niri *et al.* [13] at this juncture rely on a Monte Carlo simulation from a model of the structure to predict the signal-to-noise ratio (SNR) of each sensor *a priori*. However, this is a less practical solution for baseline subtraction techniques, and so instead a data-driven method is proposed. The only data available to help estimate the confidence of each sensor pair are the metric values computed on each waveform. By comparing the current metric value to the sensor-level threshold, "confidence factors" may be formed by computing a statistical distance from the baseline set. This method will be referred to as "NP direct scaling" fusion, and it is also described mathematically in Equation (5).

$$\mathbf{S}_{ij}^{\text{NP direct scaling}} = \begin{cases} \mathbf{D}_{ij},\ \mathbf{D}_{ij} > 1 \\ 0,\ \mathbf{D}_{ij} \le 1 \end{cases} \tag{5}$$

These confidence factors represent a kind of SNR representing by what margin a particular measurement has risen from the "noise floor" of residual energy levels that belong to the baseline set. No guarantee of optimality is given for this method because such a guarantee would have to consider the relationship between uncertainty in the input and output of the MLE first arrival estimation, which is a complicated question outside the scope of the current study. In this case, the statistical distance used is simply the ratio provided by the NRE metric, but other scaling functions are possible (for example, the number of standard deviations of the baseline NRE values from the threshold could be used). Further study to understand the propagation of uncertainty through the MLE filtering process is required to determine what the optimal scaling technique might be. However, considering that the approach utilizes the only helpful information available—that is, the comparison with threshold levels for each

pair—it is reasonable to expect it to improve performance. The data, presented below, support this supposition.

In order to apply the confidence factors correctly, prior to applying the confidence factors the minimum of each MLE filter result is subtracted from itself to make the minimum value zero. Since the MLE formulation is invariant to additive shifts, this subtraction does not impact the delay-and-sum procedure. Note that the range of values produced by the MLE filter is difficult to relate to any particular property of the underlying signal. Therefore, scaling by confidence factors does not weaken the validity of the imaging scheme in any way.

3.2. Feature Modeling

In addition to applying appropriate sensor fusion techniques, there are opportunities to add physical knowledge of the system into post-processing to further enhance detection performance. In particular, Flynn *et al.* demonstrated that for a 2D structure with a bonded stringer, implementing simple models of such geometric features can provide significant improvement in detection performance [14]. Flynn *et al.* also showed that increasing the complexity of those models further produced only marginal performance improvements. Essentially, these modeling approaches attempt to estimate the amplitude of response that should be expected for each possible damage location and then utilize that estimate to enhance the predictions. Alternatively, the models could be viewed as weighting the localization procedure according to the uncertainty in the localization estimate, because the more features the waveform crosses, the more uncertain that the result is truly representative of damage. Applying a similar approach to the current problem, simple models were developed to represent the features in each of the two testbeds in this study. Sensor fusion is also often used in combining data from sensors that are not alike, so this type of information could easily be incorporated as well, had disparate sensors been used in this study.

Direct measurement is the most straightforward way of obtaining the scattering properties of different structural features, but is not always practical in every situation. Where it is not feasible to measure, it is possible to estimate those properties through supervised learning. In this case, the model parameters were estimated by a global minimization process where the average localization error was used as the fitness function for the search. The set of damaged trials for each structure was split into “training” and “test” cases. For the frame, every fourth trial was used in training; for the fuselage rib, one case each from the first, third, and fourth hole diameters were selected, also dedicating one-fourth of the cases for training. Only these training cases were used in generated the model parameters, and to calculate the results presented in the “Localization Results” section, only test cases are used. Such a procedure is standard for machine-learning problems. Because the bolted frame has only two parameters (an attenuation coefficient and a time delay), a direct search method was computationally feasible. On the other hand, the fuselage rib’s four parameters (attenuation coefficient and time delays for both holes and stringers) necessitated the use of a genetic algorithm routine.

Calibrating the values in a *post hoc* fashion is necessary because some kind of training data is always required in SHM applications where detailed models are not available or are highly uncertain. However, similar to the previous study, the localization results are only weakly sensitive to changes in the

particular modeling parameters. In other words, merely including some recognition of the presence of geometric features is enough to realize most of the performance benefit. The impact of applying appropriate model parameters on the localization performance is presented in the "Modeling and Localization Performance" section.

3.3. Beam Spreading

Another modeling consideration that cannot be ignored in this discussion involves how a wavefront loses energy as it travels, either from material attenuation or from geometric spreading of the wave energy [15]. The material attenuation in metallic structures (typically modeled as a logarithmic decrease in wave amplitude with distance) is negligible compared to the geometric spreading [16, 17], which will be referred to here as the beam spread function. While different beam spread function models have been proposed, in a 2D medium the amplitude *B* should vary according to:

$$B = \sqrt{\frac{1}{d_{ixy} d_{jxy}}} \tag{6}$$

where d_{ixy} is the distance from the first transducer to an arbitrary scattering point, and d_{jxy} is the distance from the scattering point to the second transducer [14, 15]. For a structure composed of 1D elements, there is no beam spread effect. Such models have been shown to be beneficial in situations where estimating the expected amplitude of the scattered waveform is important. However, when this model was applied to the localization problem, the resulting prediction accuracy only deteriorated. This observation likely stems from the fact that the MLE first-arrival localization result is not directly an amplitude, but is instead a likelihood that the signal model has changed. Furthermore, the MLE result is calculated from the baseline-subtracted residual signal, which contrary to ordinary signals has a tendency to grow in time due to increasingly imprecise subtraction. Therefore, the true beam spread function, representing the expected amplitude of the residual signal, should actually be composed of two terms – one decreasing due to the energy dissipation and one increasing due to increasingly imprecise baseline subtraction. The resulting function would be difficult to estimate *a priori*, because the baseline subtraction accuracy will be geometry-dependent as well as time- (or distance) dependent. A beam spread function of unity (which is in fact the default if no such modeling is considered) produced the best results and is used for the remainder of this study.

4. Experimental Validation

In order to verify that the localization techniques developed here are generalizable to different complex structures and damage types, results from two different testbeds are considered.

4.1. Three-Story Bolted Frame Structure

The first testbed is a bolted frame structure consists of 19 elements made of 2-inch-wide by 1/8-inch-thick (5.08 cm by 3.18 mm) steel plates with 12 and 24 inch (30.5 and 61.0 cm) lengths. The elements are bolted together using steel angle brackets with two ¼-inch-diameter (6.35 mm) bolts per element. A detailed picture of the geometry is given in Figure 2.

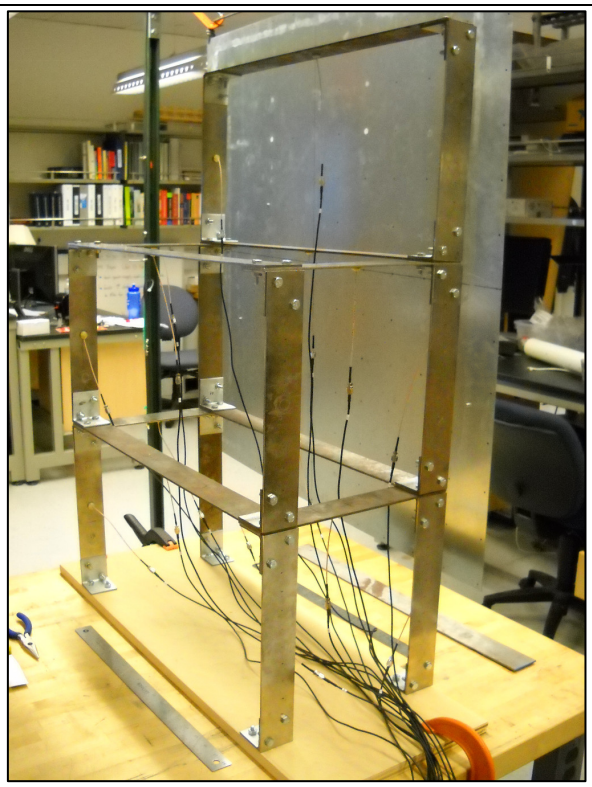

Figure 2 - Photograph of bolted frame structure

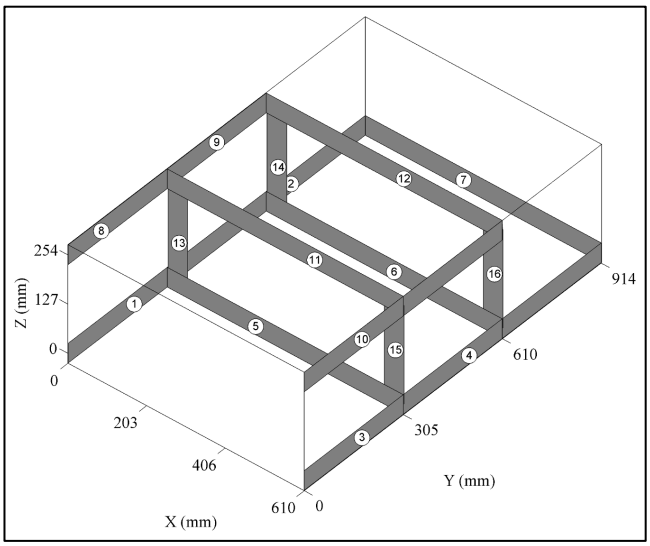

Figure 3 - Schematic of bolted frame structure showing coordinate axes and sensor locations

For this test, 16 piezoceramic sensor-actuators (PZTs) were positioned on the structure as shown in Figure 3. Note that the sensors were applied asymmetrically with the anticipation that such placement would minimize multipath ambiguity in locating the source of an arriving wave packet. The sensors were attached to a National Instruments data acquisition system, which is able to record both pitch-catch and pulse-echo modes at 2.5 MHz sampling frequency. The actuation signal used was a Gaussian-modulated sinusoid centered at 135 kHz. Each of these PZT sensors had a diameter of 12 mm, and it was determined that they produce predominantly antisymmetric (A_0) mode waves with an estimated wavelength of 25 mm.

The damage mode for this structure consisted of placing a magnet on the structure, which causes a local change in the mechanical impedance. This serves to scatter waves in such a way as corrosion or other forms of damage might, and has the benefit of being completely reversible so the performance of the algorithms might better be assessed in a controlled manner [18]. Furthermore, each of the elements for the frame structure was considered to be essentially 1D for the purposes of the wave propagation. As the magnet was nearly as wide as the element width (and was always placed in the center with respect to the element width), there is no inconsistency in making the assumption. Loss of preload in the bolted joints was considered in a past study [19]. Such damage produced very high magnitude changes that were easily detected and localized by a similar (yet less sophisticated) approach, so only magnet damage along the element is considered in the present work. Choosing thresholds in such a way as to allow no false alarms in the finite data set (consistent with the detection study), 223 of the 261 damage locations were detected. These 223 are the trials used to test the various localization algorithms.

For the frame structure, the bolted joints are the geometric features for which models were developed to play a part in the localization process. The bolted joint connections, which in the actual structure have a physical dimension, were abstracted to occur only at the point connecting the different elements. Because only damage modes along the elements were considered (i.e., damage to the bolted joints themselves was not considered), this model is sufficient to capture the relevant physics. The model consists of a simple attenuation factor and a time delay for waves passing through a joint, with all joints assumed to be identical and direction-invariant. The attenuation factor accounts for the fact that only a fraction of the incident energy will continue propagating in the forward direction. The time delay reflects the fact the wavefront will be slowed as it passes through the joint, which has a slightly longer path distance than the idealized model would indicate. Utilizing the direct search methods described previously, the best values were determined for both the NP binary and NP direct scaling fusion methods. These results are presented Table 5 in the "Modeling and Localization Performance" section.

4.2. Fuselage Rib Structure

The second testbed is a fuselage rib section from a BAe 146 aircraft. The structure is shown in Figure 4. The structure includes non-uniform thicknesses, stiffeners, and through-holes of various sizes, all of which serve as scatterers.

Six PZTs were directly applied to the top surface of the plate with cyanoacrylate adhesive in the arrangement shown in Figure 4. Note that the sensors were placed with no symmetry, and some were deliberately placed with line-of-sight obstructions to test the effect on detection performance. The excitation signal was a Gaussian-modulated sinusoid centered at 190 kHz for this test, and the sensors were used exclusively in pitch-catch mode. The PZTs had a diameter of 20 mm and were designed to excite the first symmetric Lamb wave mode (S_0) with ten times the magnitude of the first antisymmetric (A_0) mode.

Damage was introduced destructively in two modes: through-holes and simulated cracks. Holes were drilled in 4 stages, with diameters of 3.4, 4.8, 6.0, and 8.0 mm. Damage locations were selected to present increasing levels of difficulty for the sensor network to detect (i.e., further removed from the center of the sensor cluster with more intervening geometric features), as can be seen in Figure 4. Cracks were simulated by using a hacksaw to notch the stiffeners (through the whole thickness) on the reverse side of the fuselage rib. Notches were introduced in two stages, the first being about half the depth of the stiffener, and the second being the full depth.

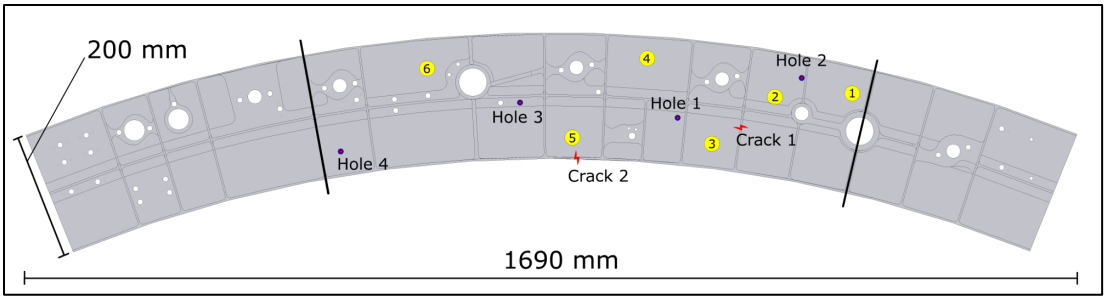

Figure 4 - Schematic of fuselage rib structure showing sensor and damage locations. The bold black lines indicate where the likelihood maps presented later are truncated for ease of viewing.

In the detection study, all of the hole damage was well-identified. Specifically, all of the damaged metric values exceeded all of the baseline metric values, except for the most remote hole at the smallest diameter, which overlapped in value with a few of the baseline cases. All of these trials are considered in the localization study. However, despite the fact that the crack damage was easily detected by the energy metric, the localization algorithms were not effective in predicting their location. This poor performance is likely because the cracks do not serve as point scatterers in the same way as the other forms of damage because the damage is not on the top surface that the sensors are on. As a result, the crack damage results are not considered here, but may be a topic for future study.

For the fuselage rib, similar energy loss coefficients and time delays to those for the bolted joints were used for the locations of significant stringers and the through-holes in the part. The values of those parameters, however, vary substantially because the stringers on this specimen are significantly less of an obstacle to guided waves than a bolted joint. While the waves in the part actually propagate around the through-holes in the specimen, these too can be considered as an attenuation coefficient and a time delay in order to simplify the model. Calibrating the parameters yielded the values found in Table 6 in the "Modeling and Localization Performance" section.

5. Localization Results

The localization for both structures was carried out using identical processes. The only algorithm inputs that differed were geometry-related or related to the different data acquisition systems used to collect the data. Using identical procedures ensures that the localization strategy is truly generalizable, although usually some structure-specific information is beneficial for improving the system performance.

5.1. Localization Performance Comparisons

First, a comparison of the proposed approach with other localization techniques from the literature is presented in order to further validate the maximum likelihood estimation approach to sparse array localization. A similar comparative study was performed by Flynn *et al*. previously [5], and the current list of methods is the same except for the addition of the MVDR method. A brief description and references are given here for each method – for more details, the reader is referred to Flynn *et al*. or the references given here.

All methods operate on the data filtered about the input frequency band and optimally baseline-subtracted. Each signal is also enveloped by taking the magnitude of the Hilbert transform unless otherwise mentioned. The WTOA, TDOA, and WTP methods all use an exponential window on the data, where the time constant was chosen as 80 μs for the fuselage rib and 200 μs for the frame structure (according to the approximate ratio of group velocities). The compared methods are reviewed briefly here:

TOA – the time of arrival method or the ellipse method is the most basic approach, simply computing the delay-and-sum result for the enveloped waveform. [20]

WTOA – the windowed time of arrival method adds an exponential time window to the TOA method in order to suppress later reflections. Because the boundary reflections and inaccurate baseline subtraction effects become more and more dominant with time, the purpose of the exponential time window is to mitigate those effects by giving the information earlier in the signal a relatively higher weighting.

TDOA – the time difference of arrival method is based on correlations between each two sensor pairs that have exactly one sensor in common. This method is commonly used for source localization using passive systems, since the algorithm does not require knowledge of the time origin of the source signal. For the cross-correlations, an exponential window was also applied to the data. Because the method operates on two sensor pairs simultaneously, the fusion approaches are not implemented to avoid a potentially false comparison. [21]

RAPID – the reconstruction algorithm for the probabilistic inspection of damage is based on the zero-lag cross-correlation of the baseline and test signals (without enveloping). The results for each transducer pair are then computed over elliptical sub-regions, the size of which is controlled by a factor beta. The additional beta parameter was calibrated in post-processing to maximize the localization accuracy and set to a value of 1.45, with a time window of 50 μs. [22]

EA – the energy arrival method is based on calculating the energy in a time window beginning at the estimated arrival time (without enveloping the signal first). The resulting value is then inversely weighted, in effect, by the amount of energy before the estimated arrival time. This formulation is similar to the MLE approach in that it is looking for a time point where the previous energy is minimized compared to the energy in the window, but it differs in that it does not consider the reflections occurring after the narrow time window. [23]

TP – the total product method is based on taking the product of the short-time Fourier transform of each sensor pair's waveform, computed at the actuation frequency and centered on the expected arrival time. As was previously noted by Flynn *et al*., this is approximately equivalent to the product of the each sensor pair's waveform (after filtering and enveloping) at the expected arrival time for each point on the structure, and therefore the simpler implementation has again been adopted. Furthermore, because this technique is multiplicative, applying weighting factors to the sensor pairs does not change the result. Therefore, there is no difference in this method between NP binary and NP direct scaling fusion techniques. [24]

WTP – the weighted total product method adds an exponential time window to the TP method.

MVDR – the minimum variance distortionless response method attempts to compute a set of optimal weights such that the energy that is not present in the "look direction" of any given pixel is minimized. The objective of this approach is to minimize imaging artifacts not in the given look direction. Phase information, dispersion compensation, and scattering fields may also be integrated directly into the approach where appropriate and when such information is available. However, to perform a fair comparison with the other techniques presented, none of these options were used. Beam speading is typically included in the computation of the initial "steering vectors" according to Equation 6. While it was not implemented for the frame structure to better represent the physics, for the fuselage rib the method was found to perform marginally better including the beam spread effect, and it has been included. Furthermore, the MVDR method is already optimizing over the look vector, which is analogous to the sensor weighting provided by the sensor fusion techniques, so the direct scaling approach was not implemented. [25]

Table 1 - Comparison of localization algorithms in bolted frame structure (all trials)

Frame Structure - Mean Prediction Error (mm)									
MLE	**TOA**	**WTOA**	**TDOA**	**RAPID**	**EA**	**TP**	**WTP**	**MVDR**	**Fusion Technique**
250	1019	730	624	636	926	1010	743	423	All PC channels
132	1004	645	-	222	943	1077	391	612	NP binary
120	970	614	-	141	747	-	-	-	NP direct scaling

Table 1 gives a comparison of the different localization algorithms for the frame structure with no feature modeling applied. For this purpose, taking the distance between the predicted location and the true damage location provides a convenient and descriptive measure of the localization accuracy for quantitative comparison. Both the results for the NP binary fusion and NP direct scaling fusion methods are presented, along with the results for using all pitch-catch sensor pairs. For those methods where the fusion method chosen either does not influence the results or is undefined, only one entry is made. For a structure of this complexity, the TOA, EA, and TP methods are unable to outperform the completely uninformed localizer, which for the frame structure produces a mean error of 644 mm (as presented later in Table 5). (The uninformed localizer is one given no information on the damage location, so the best damage prediction possible is to always predict the "geometric centroid" of the structure, which is to say whatever point is closest, on average, to every other possible damage location.) The MLE formulation works the best, with only the RAPID and WTP methods approaching the level of performance achieved by MLE. Also note that in every case, the NP direct scaling fusion improved localization performance over that obtained by the NP binary fusion.

Table 2 - Comparison of localization algorithms in fuselage rib structure (all trials)

Fuselage Rib Structure - Mean Prediction Error (mm)									
MLE	**TOA**	**WTOA**	**TDOA**	**RAPID**	**EA**	**TP**	**WTP**	**MVDR**	**Fusion Technique**
194	573	339	296	336	259	473	303	414	All PC channels
74	601	309	-	149	188	630	337	382	NP binary
63	443	324	-	141	163	-	-	-	NP direct scaling

Table 2 presents the comparison of the localization algorithms for the fuselage rib structure, again with no feature modeling. Again, the MLE formulation performs the best, this time by a factor of more than two (in terms of mean prediction error) over the second-best method. The second-best method for each structure is the RAPID technique, while none of the other methods performed well on both of the structures tested.

To more completely visualize the performance of each algorithm, localization performance curves are computed. Rather than simply giving the average localization error, these plots express the fraction of damage cases had an error less than a specific bound. They may be interpreted similar to receiver operating characteristic curves, in that the ideal localizer should produce a square curve in the top left corner. Results for the bolted frame structure are given in Figure 5 and the corresponding plot for the fuselage rib is given in Figure 6.

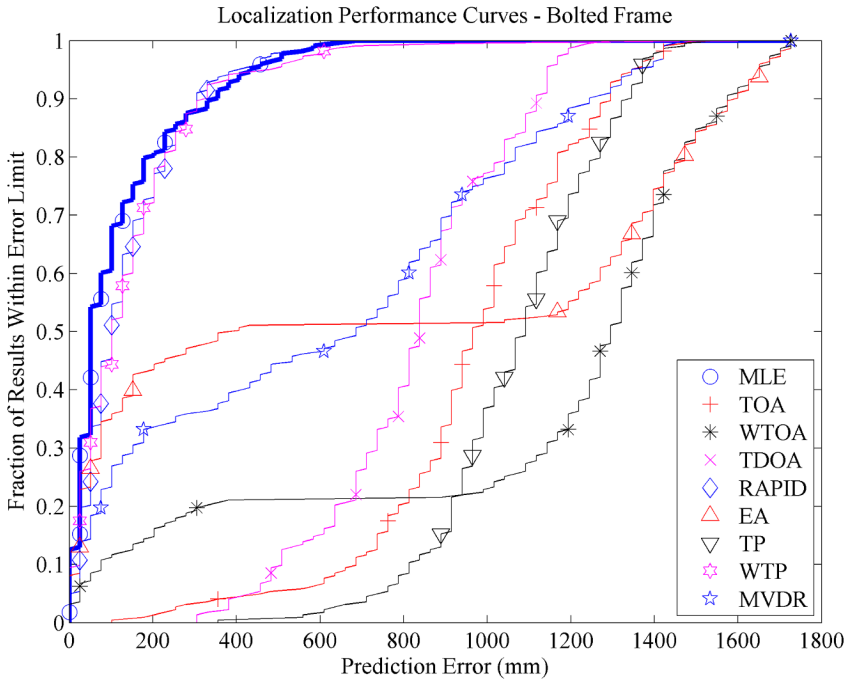

Figure 5 - Localization performance curves for the bolted frame structure. NP direct scaling fusion, no feature modeling.

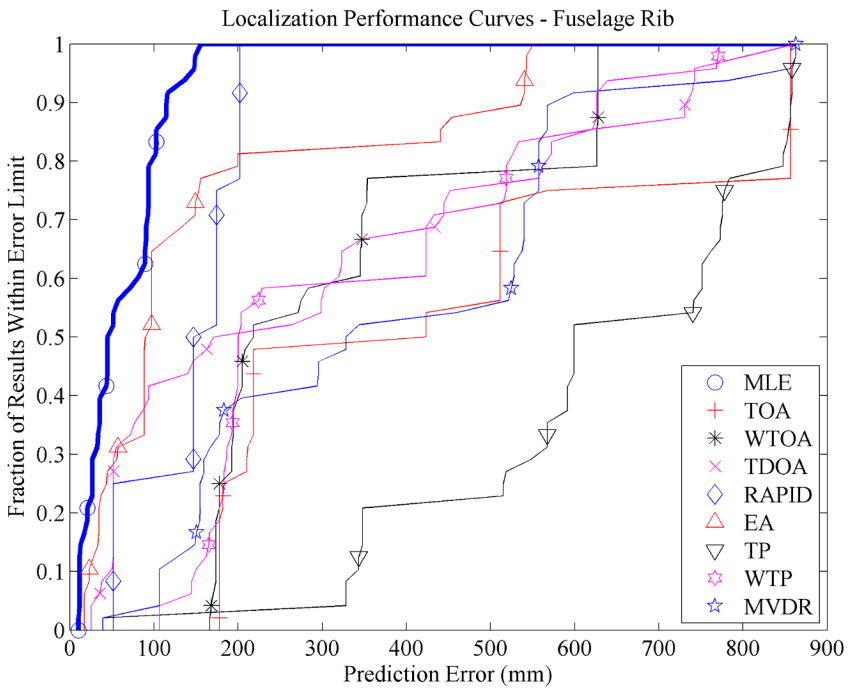

Figure 6 - Localization performance curves for the fuselage rib structure. NP direct scaling fusion, no feature modeling.

To further quantify these localization performance curves, an area-under-the-curve (AUC) metric may be implemented by integrating from zero to the maximum error and then normalizing such that perfect localization produces a value of one. The comparison results are again presented using this metric in Table 3 and Table 4.

Table 3 - Normalized AUC metric comparison for all localization algorithms in the frame structure (all trials)

Frame Structure - Normalized AUC									
MLE	**TOA**	**WTOA**	**TDOA**	**RAPID**	**EA**	**TP**	**WTP**	**MVDR**	**Fusion Technique**
0.857	0.412	0.580	0.641	0.633	0.466	0.417	0.572	0.757	All PC channels
0.925	0.420	0.629	-	0.874	0.456	0.378	0.776	0.647	NP binary
0.931	0.440	0.647	-	0.919	0.570	-	-	-	NP direct scaling

Table 4 - Normalized AUC metric comparison for all localization algorithms in the fuselage rib structure (all trials)

Fuselage Rib Structure - Normalized AUC									
MLE	**TOA**	**WTOA**	**TDOA**	**RAPID**	**EA**	**TP**	**WTP**	**MVDR**	**Fusion Technique**
0.785	0.346	0.615	0.667	0.618	0.709	0.462	0.657	0.529	All PC channels
0.921	0.313	0.648	-	0.832	0.788	0.280	0.617	0.567	NP binary
0.929	0.495	0.630	-	0.838	0.818	-	-	-	NP direct scaling

All three methods of comparing the different localization procedures suggest the same conclusion – the MLE procedure produces the most accurate results. The RAPID method performs second-best, and no other method is able to produce comparable results for both testbeds. These conclusions hold whether all sensor pairs are considered, or whether the NP binary or direct scaling fusion methods are applied.

5.2. Modeling and Localization Performance

With the MLE first arrival localization approach having been validated for the proposed application, the next step is to test the performance of the proposed sensor fusion and modeling approaches. Table 5 and Table 6 show results for the MLE formulation with different sensor fusion and modeling strategies implemented. Runs 100 and 200 represent the performance with no localization information (i.e. simply picking the geometric centroid each time) for a reference. Next, the results using all pitch-catch (PC) channels is presented, followed by the results obtained by using the location of the sensor receiving the most votes in the sensor-by-sensor detection threshold process. These two methods are also presented as a baseline for the performance an intelligent SHM system should exceed. It should be noted that without appropriate sensor fusion techniques (as in the case of 101 and 201), the ellipse methods of localization for such complex structures are very inaccurate, and methods not based on delay and sum (as for 102 and 202) can be more accurate. Finally, results are presented for NP binary fusion and NP direct scaling fusion, both with and without the feature modeling parameters obtained as described previously. For simplicity, the feature modeling parameters were calculated using the NP direct scaling only and kept constant for both of the fusion methods presented here. These tables are calculated using only the trials designated as "test", so as not to bias the model parameter estimation. The results in the previous section were presented for all trials, which accounts for the minor discrepancies in some parallel results. Both the average prediction error and the AUC metric are presented for each case.

Table 5 - Mean localization error for bolted frame structure (MLE formulation with different modeling and fusion techniques)

Frame Structure			Model Parameters		
Run #	Mean Error (mm)	AUC	Delay (μs)	Attenuation	Fusion Technique
100	649	0.562	0	1	Centroid (no info)
101	251	0.832	0	1	All PC channels
102	133	0.911	0	1	Most popular sensor
103	136	0.911	0	1	NP binary
104	121	0.919	0	1	NP direct scaling
105	69.4	0.955	5.8	0.595	NP binary
106	65.4	0.957	5.8	0.595	NP direct scaling

Table 6 - Mean localization error for fuselage rib structure hole damage (MLE formulation with different modeling and fusion techniques, all test cases)

Fuselage Rib Structure			Model Parameters [Hole, Stringer]		
Run #	Mean Error (mm)	AUC	Delay (μs)	Attenuation	Fusion Technique
200	254	0.703	[0, 0]	[1,1]	Centroid (no info)
201	196	0.780	[0, 0]	[1,1]	All PC channels
202	140	0.838	[0, 0]	[1,1]	Most popular sensor
203	78.9	0.916	[0, 0]	[1,1]	NP binary
204	59.6	0.931	[0, 0]	[1,1]	NP direct scaling
205	72.5	0.922	[1.44, 0.010]	[0.995, 0.995]	NP binary
206	56.2	0.936	[1.44, 0.010]	[0.995, 0.995]	NP direct scaling

For both the frame and rib structures, the implementation of some form of feature modeling produced a drop in the localization error, which was very significant for the frame structure. The fuselage rib structure benefitted less from the feature modeling, most likely because there are many more intervening features (which were actually inhomogeneous), making model parameters more imprecise. NP direct scaling also outperformed NP binary sensor fusion in all cases, just as both of those techniques outperformed the results using all sensor pairs. The final value for the average localization error in the frame structure was a mere 65 mm, compared to a maximum path distance in the structure of 1.8 meters. The wavelength for this structure is about 25 mm, and getting an average error about 2.5 times the wavelength value is an excellent result. The results in the fuselage rib structure are similarly excellent, with the average error decreasing from 196 mm with no sensor fusion or feature modeling down to just 56 mm when NP direct scaling and feature modeling were implemented.

As mentioned previously, the localization error is not strongly sensitive to small fluctuations in the model parameters – for example, attenuation values from 0.25 to 0.80 (depending on the time delay) yielded results within 10% of the minimum error for the bolted frame. This further removes the need to create detailed models – estimated parameters are likely sufficient to capture the majority of the benefit.

5.3. Localization Figures

Now that the optimal localization procedure has been established, a final graphical view of the results is presented. The following damage localization figures are maps of the likelihood that the damage (which has been detected already, as previously noted) is at a given point on the structure. Therefore, the location of the maximum likelihood is taken to be the predicted damage location. Sensors are plotted as white circle with the corresponding channel number. For convenience, the log-likelihood values output from the algorithm have been normalized to a linear scale between 0 and 1. However, it should be noted that these values do not represent a probability in any sense, only a normalized likelihood which is useful for visualizing why a particular maximum point was selected. These maps are also not meant to represent damage maps directly, and they cannot be used to estimate the size or extent of damage.

Two damage likelihood maps (of the 223 total) were chosen as representative examples. Figure 7 shows an example where the damage location estimate directly coincided with the prediction. Note that the likelihood values are highest on the element containing the damage, dramatically lower on the other elements, and tend to decrease with distance from the damage – all as would be expected for a good localization procedure. Figure 8 is an example of a less accurate estimation. In that case, the damage was located on an element on which no sensor was placed, a situation that tended to produce higher estimation errors (again, as expected). The accuracy of the localization is dependent on the part of the structure in which the damage occurs. This effect is due to the fact that the coverage is not uniform – damage toward the center of the structure will disrupt the signal between more sensor pairs, whereas some elements are without a sensor at all.

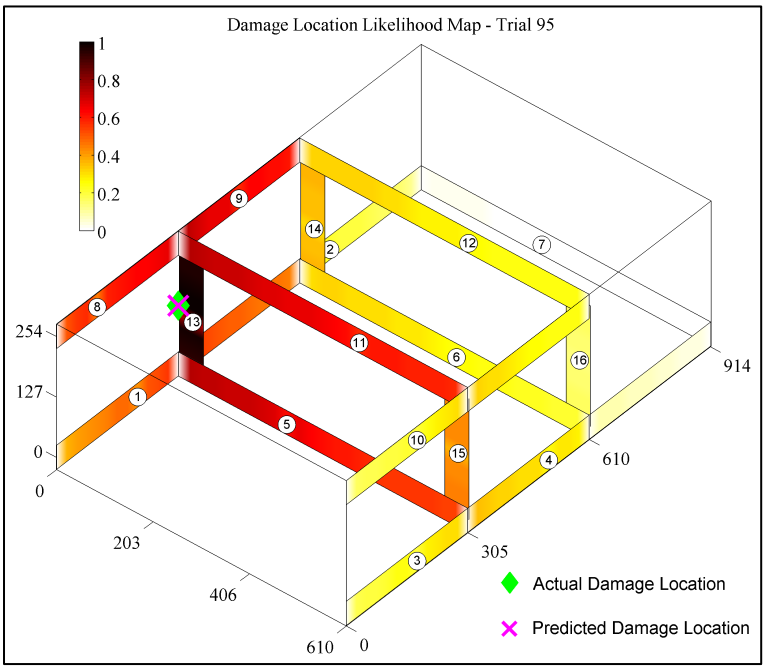

Figure 7 - Damage likelihood map, frame structure trial 95 (all dimensions given in mm)

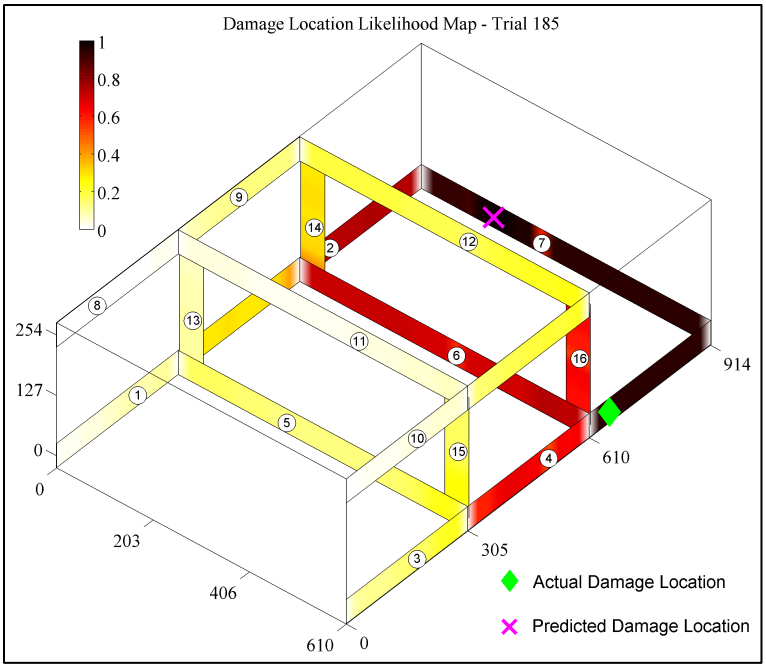

Figure 8 - Damage likelihood map, frame structure trial 185 (all dimensions given in mm)

For the fuselage rib structure, black circles represent through-holes in the part, where the solid black lines represent the larger stringers behind the instrumented surface. This represents a simplification of the part's actual geometry—smaller stringers and thickness changes were not considered for simplicity. Again, the likelihood values were normalized to fall between 0 and 1, where 1 represents the predicted damage location.

One example from each hole location on the fuselage rib is presented (each at the maximum hole diameter). The first two hole locations, shown in Figure 9 and Figure 10, are centrally located with respect to the sensor array and are therefore located very accurately. Figure 11 shows a hole location that is obscured from the direct line of sight of the closest sensors by through-holes, and the likelihood map is distorted in that region because the localization algorithm considers the obstacle. Similar distortions may be observed around the features in each of the likelihood maps. Finally, Figure 12 depicts hole location 4, which is well outside of the sensor array. Because the array viewed from that angle is nearly linear, the range to the damage can be predicted well, but the angular component is unreliable. As a result, there is a roughly elliptical band of high likelihoods with nearly the correct range, but the predicted position fluctuates within that band, causing a higher prediction error to be observed for the last hole location.

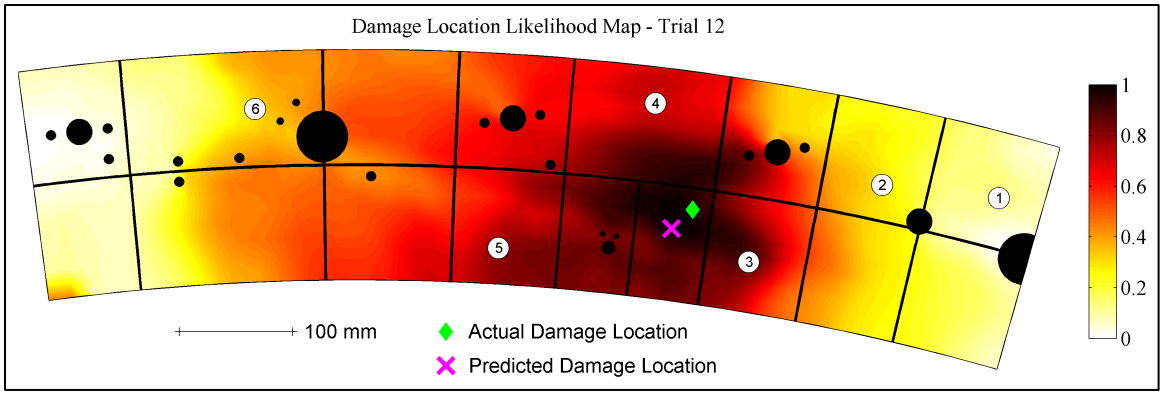

Figure 9 - Damage likelihood map, fuselage rib, first hole location

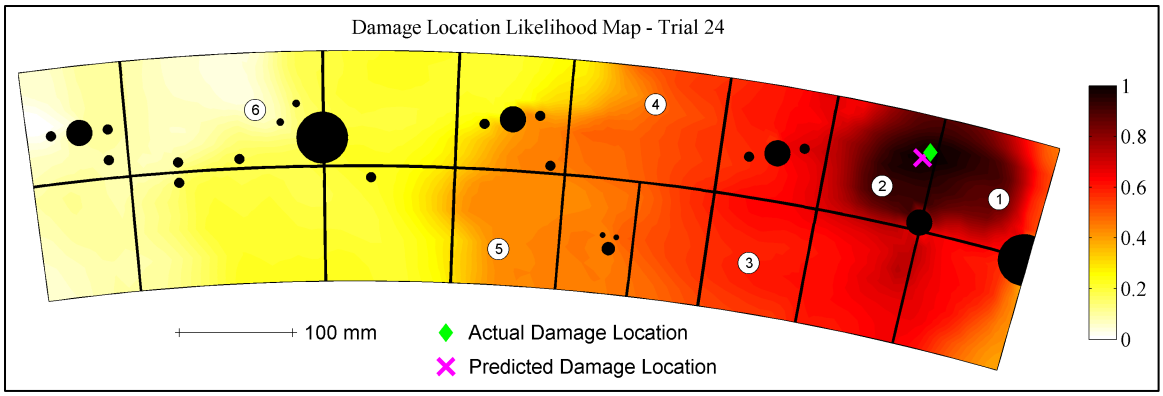

Figure 10 - Damage likelihood map, fuselage rib, second hole location

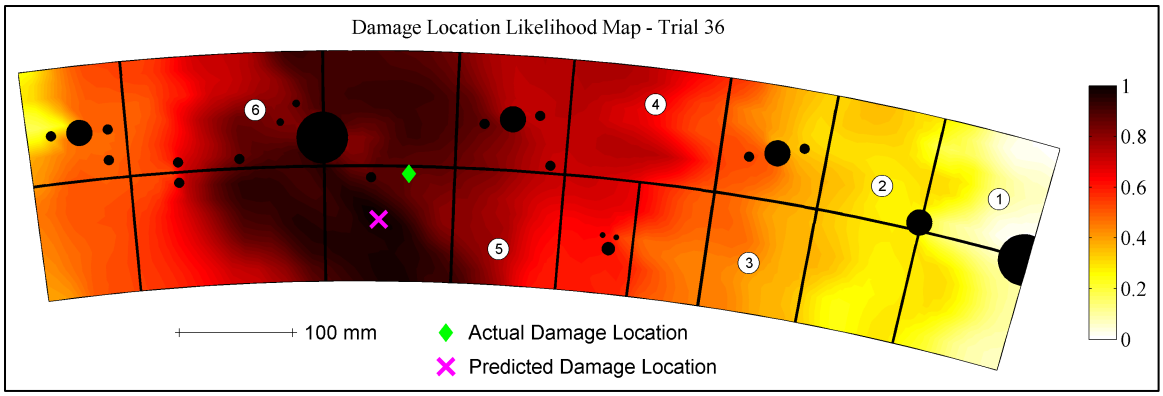

Figure 11 - Damage likelihood map, fuselage rib, third hole location

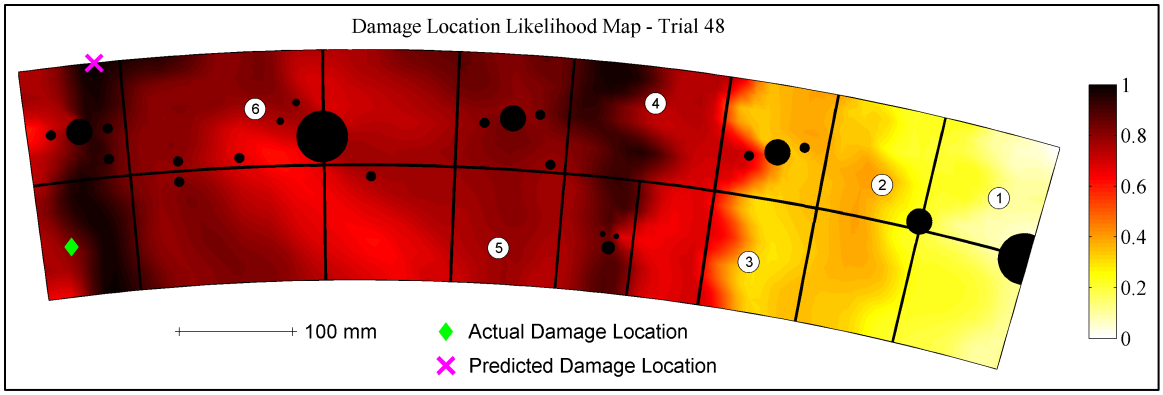

Figure 12 - Damage likelihood map, fuselage rib, fourth hole location

6. Conclusion

A statistical approach to localization which is applicable to highly-complex structures has been presented and validated. Two dissimilar structures with different modes of single-site, simulated damage were used to conduct a detailed comparison between different delay-and-sum imaging approaches in the literature. The maximum likelihood estimation approach outperformed all of the other approaches to which it was compared. To further improve the localization performance, a novel approach to the sensor fusion process was then developed based upon applying the Neyman-Pearson criterion to each sensor pair and weighting contributions according to their sensor-level thresholds. In order to explicitly consider the impact of the geometry on localization, simple models were developed for bolted joints, stringers, and holes in each specimen. Including the sensor fusion and geometric modeling steps in the localization procedure further enhanced the estimation accuracy, reducing the average error by 74% for the bolted frame and 71% for the fuselage rib over using the MLE approach alone.

This work illustrates the importance of developing SHM techniques specifically designed for structures of realistic complexity. While many challenges still remain, one of the chief hindrances for ultrasonic SHM systems has been the multi-path interference and scattering from non-damage reflectors which can make the signals difficult to interpret. The demonstrated improvement in localization performance given by the proposed techniques represents a significant step toward overcoming these obstacles and making SHM feasible in application.

Acknowledgments

This work was primarily supported by the National Science Foundation through a Graduate Research Fellowship (Colin Haynes). This research was also performed under grant #UG110097JD of the Agency for Defense Development in Korea by the Leading Foreign Research Institute Recruitment Program (2011-0030065) through the National Research Foundation of Korea, funded by the Ministry of Education, Science, and Technology (Korea). The authors would like to acknowledge the University of Bristol (UK) NDT Laboratory for providing the fuselage rib experimental testbed and hosting that set of experiments.

References

1. A. Rytter, Vibration based inspection of civil engineering structures, 1993,.

2. K. Worden, C.R. Farrar, G. Manson, G. Park, The fundamental axioms of structural health monitoring, Proc. R. Soc. Math. Phys. Eng. Sci. 463, 2082; 2007, 1639–1664.

3. A.J. Croxford, P.D. Wilcox, B.W. Drinkwater, G. Konstantinidis, Strategies for guided-wave structural health monitoring, Proc. R. Soc. Math. Phys. Eng. Sci. 463, 2087; 2007, 2961–2981.

4. C. Haynes, M.D. Todd, E. Flynn, A. Croxford, Statistically-based damage detection in geometrically-complex structures using ultrasonic interrogation, Struct. Health Monit. 12, 2; 2013, 141–152.

5. E.B. Flynn, M.D. Todd, P.D. Wilcox, B.W. Drinkwater, A.J. Croxford, Maximum-likelihood estimation of damage location in guided-wave structural health monitoring, Proc. R. Soc. Math. Phys. Eng. Sci. 467, 2133; 2011, 2575–2596.

6. T. Clarke, P. Cawley, Enhancing the defect localization capability of a guided wave SHM system applied to a complex structure, Struct. Health Monit. 10, 3; 2011, 247–259.

7. C.T. Ng, M. Veidt, A Lamb-wave-based technique for damage detection in composite laminates, Smart Mater. Struct. 18, 7; 2009, 074006.

8. C.H. Wang, J.T. Rose, F.-K. Chang, A synthetic time-reversal imaging method for structural health monitoring, Smart Mater. Struct. 13, 2; 2004, 415.

9. A.J. Croxford, J. Moll, P.D. Wilcox, J.E. Michaels, Efficient temperature compensation strategies for guided wave structural health monitoring, Ultrasonics. 50, 4-5; 2010, 517–528.

10. David L. Hall, Mathematical Techniques in Multisensor Data Fusion, Artech House, Boston, 1992.

11. Q. Liu, H. Wang, A case study on multisensor data fusion for imbalance diagnosis of rotating machinery, Artif Intell Eng Anal Manuf. 15, 3; 2001, 203–210.

12. Y. Lu, J.E. Michaels, Feature Extraction and Sensor Fusion for Ultrasonic Structural Health Monitoring Under Changing Environmental Conditions, IEEE Sens. J. 9, 11; 2009, 1462–1471.

13. E.D. Niri, A. Farhidzadeh, S. Salamone, Adaptive multisensor data fusion for acoustic emission source localization in noisy environment, Struct. Health Monit. 12, 1; 2013, 59–77.

14. E.B. Flynn, M.D. Todd, A.J. Croxford, B.W. Drinkwater, P.D. Wilcox, Enhanced detection through low-order stochastic modeling for guided-wave structural health monitoring, Struct. Health Monit. 11, 2; 2012, 149–160.

15. P.D. Wilcox, M.J.S. Lowe, P. Cawley, Mode and Transducer Selection for Long Range Lamb Wave Inspection, J. Intell. Mater. Syst. Struct. 12, 8; 2001, 553–565.

16. R.P. Dalton, P. Cawley, M.J.S. Lowe, The Potential of Guided Waves for Monitoring Large Areas of Metallic Aircraft Fuselage Structure, J. Nondestruct. Eval. 20, 1; 2001, 29–46.

17. Lester W. Schmerr, Jr., Fundamentals of ultrasonic nondestructive evaluation: a modeling approach, Plenum Press, New York, 1998.

18. E.B. Flynn, M.D. Todd, Optimal Placement of Piezoelectric Actuators and Sensors for Detecting Damage in Plate Structures, J. Intell. Mater. Syst. Struct. 21, 3; 2010, 265–274.

19. C.M. Haynes, M.D. Todd, Bayesian probabilistic modeling for damage assessment in a bolted frame, Proc. SPIE, 2012,, San Diego, CA.

20. J.E. Michaels, T.E. Michaels, Guided wave signal processing and image fusion for in situ damage localization in plates, Wave Motion. 44, 6; 2007, 482–492.

21. J.E. Michaels, A.J. Croxford, P.D. Wilcox, Imaging algorithms for locating damage via in situ ultrasonic sensors, Proc. IEEE Sens. Appl. Symp. 2008 SAS 2008, 2008, 63–67,

22. H. Gao, Y. Shi, J.L. Rose, Guided Wave Tomography on an Aircraft Wing with Leave in Place Sensors, Proc. AIP Conf. Proc., 760, 2005, 1788–1794,

23. J.E. Michaels, T.E. Michaels, Damage Localization in Inhomogeneous Plates Using a Sparse Array of Ultrasonic Transducers, Proc. AIP Conf. Proc., 894, 2007, 846–853,

24. J.-B. Ihn, F.-K. Chang, Pitch-catch Active Sensing Methods in Structural Health Monitoring for Aircraft Structures, Struct. Health Monit. 7, 1; 2008, 5 –19.

25. J.S. Hall, J.E. Michaels, Minimum variance ultrasonic imaging applied to an in situ sparse guided wave array, IEEE Trans. Ultrason. Ferroelectr. Freq. Control. 57, 10; 2010, 2311 –2323.